Journal of Thermal Engineering *http://eds.yildiz.edu.tr/journal-of-thermal-engineering/Articles*
Yildiz Technical University Press, Istanbul, Turkey *Manuscript Received May 28, 2015; Accepted September 11, 2015*
Vol. 2, No. 2, pp. 761-773, July, 2016.

This paper was recommended for publication in revised form by Editor in Chief Ahmet Selim Dalkilic

FLOW BOILING HEAT TRANSFER IN A RECTANGULAR COPPER MICROCHANNEL

Mehmed R. ÖZDEMİR*
Brunel University London
College of Engineering, Design and Physical Sciences, UK
Marmara University Mechanical Engineering Department
Istanbul, TURKEY

Mohamed M. MAHMOUD
Brunel University London
College of Engineering, Design and Physical Sciences, UK
Faculty of Engineering Zagazig University
Sharqia, EGYPT

Tassos G. KARAYIANNIS
Brunel University London
College of Engineering, Design and Physical Sciences, UK

Keywords:flow boiling, microchannel, heat transfer coefficient, flow patterns, instability
** Corresponding author:Mehmed Rafet Özdemir*
E-mail address:mehmed.oezdemir@brunel.ac.uk

ABSTRACT

Flow boiling characteristics of de-ionized water were tested experimentally in a rectangular copper single microchannel of 1 mm width, 0.39 mm height and 62 mm length. De-ionized water was supplied to the microchannel at constant inlet temperature (89°C) and constant inlet pressure (115 kPa). The mass flux ranged from 200 to 800 kg/m^{2}s and the heat flux from 56 to 865 kW/m^2. The heat transfer rate data are presented as plots of local heat transfer coefficient versus vapour quality and distance along the channel. Flow visualization was also conducted using a high-speed, high-resolution camera. The results indicate that unstable flow boiling occurred starting at boiling incipience for all mass flux values. The local heat transfer coefficient depends on heat flux only at very low heat and mass fluxes. At high mass flux, there is no heat flux effect with little dependence on vapour quality after the entry region. The mass flux effect was more complex.

INTRODUCTION

Rapid developments in miniaturization and performance of electronics devices resulted in a significant challenge in the thermal management of these devices. The heat dissipation rate from these high performance and compact devices reached huge values and consequently the traditional cooling methods such as air cooling became ineffective. For example, as cited in ref. [1], the heat flux in applications such as high power laser, microwave devices and radars exceeds 10 MW/m^2. Microchannel heat sinks are one of the proposed methods for cooling these high heat flux devices. Kandlikar [2] reported that heat dissipation rate as high as 10 MW/m^2 is possible using single phase flow in microchannel heat sinks with enhanced surface. However, this could be accompanied by excessive pressure drop and non-uniform temperature distribution in the electronic chip. On the contrary, flow boiling in microchannel heat sinks can achieve high heat transfer rates, better axial temperature uniformity, low mass flow rates and low pressure drop or less pumping power than single phase flow [3, 4]. Two phase flow microchannel heat exchangers can be used in various applications other than electronics cooling such as cooling turbine blades, rocket engine, refrigeration cooling, microprocessors, laser diodes, aviation, biomedical applications and densely packed integrated circuits [5-7]. However, there are some limitations in applying this method including the early dryout and flow instabilities that can cause catastrophic failure of the electronic devices [8, 9]. Also, flow boiling characteristics in microchannel heat sinks are still not completely understood with many experimental studies concluding contradicting results. The reasons for these contradictions could be due to the variation in the surface characteristics and different heated lengths of the tested channels [10-12] and flow instabilities [3]. A brief review on flow patterns, flow instability and heat transfer rate in single and multi-microchannels is given below to introduce some aspects relevant to this study. It is worth mentioning that, few researchers performed flow boiling in a single rectangular microchannel. Thus, the review included also

studies on multi-microchannel heat sinks to enable a broad understanding in the topic.

Flow Patterns

Flow visualization in microchannels is important due to its direct link with heat transfer characteristics and pressure drop. The commonly observed flow patterns in large diameter horizontal channels are bubbly, slug, plug, annular, stratified, annular-mist and wavy flow as reported by Thome [13]. According to Kandlikar [14], the dominant flow patterns in microchannels are isolated bubble, confined bubble/slug and annular flow. Several researchers [15-18] studied flow boiling patterns in microchannels. For example, Sobierska et al. [15] performed experiments using water in a single copper vertical rectangular microchannel with hydraulic diameter D_h = 1.2 mm and aspect ratio W/H = 0.43. The total length of the channel was 330 mm and flow visualization was conducted at five locations along the channel. They reported three flow patterns namely bubbly, slug and annular flow but they did not mention where exactly these flow patterns were observed along the channel. It is worth mentioning that bubbly flow was observed under subcooled conditions, i.e. fluid bulk temperature is below saturation. The inlet subcooling was varied from 2 to 20 K. Megahed and Hassan [16] carried out experiments with FC-72 in silicone rectangular multi-microchannels having hydraulic diameter 0.247 mm, aspect ratio W/H = 0.82, and 16 mm length. Flow visualization was conducted at three locations along the transverse direction at the middle of the heat sink and also near the channel exit. The flow patterns reported at one heat flux value of 130.6 kW/m^2 and mass flux of 341 kg/m^{2}s demonstrated that the flow patterns observed along the transverse direction are different. Slug flow was observed in the central channels while wispy-annular flow was observed in the extreme side channels. This indicates that the flow was not uniformly distributed among the channels. Near the channel exit, three main flow patterns were observed in the central channels, namely bubbly, slug and annular flow.

Chen and Garimella [17] conducted a visualization study on flow boiling of FC-77 in silicone multi-microchannels with 0.389 mm hydraulic diameter, aspect ratio 1 and 12.7 mm length over a range of heat flux (40 – 730 kW/m^2) and at three different mass flux (332, 446 and 570 kg/m^{2}s). Visualization was conducted near the channel exit at the centerline of the heat sink. They reported that bubbly flow is dominant at low heat flux while bubbles grow and merge faster as heat flux increases resulting in slug flow at intermediate heat flux. As heat flux increased further, alternating wispy-annular flow and churn flow were observed. At these conditions, when the camera was moved to the channel inlet region, flow reversal was observed. Thus, the formation of alternating wispy-annular and churn flow was attributed to the occurrence of flow reversal [17]. Balasubramanian et al. [18] investigated de-ionized water flow boiling in copper rectangular multi-microchannels with hydraulic diameter D_h = 0.342 mm, aspect ratio W/H = 0.167 and two channel lengths 25 and 20 mm. They observed dispersed bubble, intermittent (slug and elongated bubble) and annular flows in their study. In the intermittent flow regime, bubbles nucleate and grow rapidly to the channel size before detaching from the wall with many bubbles nucleating from the side walls.

Flow Instabilities

Flow boiling instability is one of the limitations in microchannel heat exchangers. Identifying the operating conditions of stable flow boiling is very important for the reliable design of micro heat exchangers. Some researchers [19-25] investigated flow boiling instability in microchannels. Qu and Mudawar [19] investigated pressure drop and hydrodynamic instability of water flow boiling in a copper multi-microchannel heat sink having hydraulic diameter 0.35 mm, aspect ratio W/H = 0.32 and 44.8 mm channel length. They reported severe pressure drop oscillations at boiling incipience. This was attributed to the presence of a compressible volume in the upstream side of the test section. The authors also reported that this kind of instability results in pre-mature critical heat flux (CHF). They managed to suppress this pressure drop instability using a throttling valve located before the test section inlet. Chang and Pan [20] investigated experimentally flow boiling instability of water in a silicon-based multi-microhannel heat sink having 0.0863 mm hydraulic diameter, 1.3 aspect ratio (W/H) and 42 mm channel length over a heat flux range 7.68 – 87.7 kW/m^2 and mass flux range 22 – 110 kg/m^{2}s. They presented flow patterns captured along the centerline of the heat sink near the inlet, middle and near the outlet at mass flux 22 kg/m^{2}s at different heat flux. Instability due to boiling incipience was not observed. At the lowest heat flux and near the channel inlet, small nucleating bubbles were observed in some of the channels while near the channel exit the flow pattern was varying between slug and annular flow. However, when increasing the heat flux to 15.8 kW/m^2, unstable flow was observed. In this case the flow was alternating between slug and annular flow with back and forth motion and large amplitude pressure drop oscillation. The pressure drop oscillation corresponding to the stable case was less than 6 kPa while it was greater than 6 kPa and up to 23 kPa for the unstable case. Bogojevic et al. [21] carried out an experimental study with water to investigate flow boiling instabilities in silicone based multi-microchannels with 0.194 mm hydraulic diameter, aspect ratio W/H = 0.55 and 15 mm length. Two inlet sub-cooling degrees were tested (29 K and 75 K) over mass flux range 41.7 – 433.3 kg/m^{2}s and heat flux range 178 – 445 kW/m^2. The stability/instability criterion was chosen as the oscillation in

the measured pressure and temperature. They reported two kinds of instability namely high amplitude low frequency (HALF) with a frequency range 0.9 – 2.88 Hz and low amplitude high frequency (LAHF) with a frequency range 23 – 25 Hz. Their results demonstrated that flow instability depends on the ratio of heat to mass flux (q''/G) and the inlet subcooling degree. For the high inlet sub-cooling test (75 K), stable flow occurred for q''/G < 2.62 kJ/kg while for the lowest inlet sub-cooling test (29 K) stable flow occurred for q''/G < 0.99 kJ/kg. Additionally, It was concluded that, the lower the inlet subcooling (high fluid inlet temperature), the lower the magnitude of temperature oscillation. Wang et al. [22] investigated experimentally flow boiling instabilities of water in silicon multi-microchannels and in a single channel at 35 °C inlet temperature. Both test sections had an identical trapezoidal cross section with 186 μm hydraulic diameter and 30 mm length. They presented their data similarly as Bogojevic et al. [21] and defined two modes of unstable boiling. The first mode is long period oscillation (more than 1 s) while the second is short period oscillation (less than 0.1 s). The unstable mode with long period oscillation occurred for 0.96 kJ/kg < q''/G < 2.14 kJ/kg in the multi-microchannels and for 0.09 kJ/kg < q''/G < 0.32 kJ/kg in the single microchannel. However, unstable flow boiling mode with short period oscillation occurred for q''/G > 0.32 kJ/kg and q''/G > 2.14 kJ/kg in the single and multi-microchannels, respectively. In the long period oscillation instability mode they indicated that the oscillation period of temperature in the single microchannel (10 - 80 ms) was much longer than that in the multi-microchannels (2.5 - 9.8 ms) at the same heat flux. Additionally, in the short period oscillation mode they observed that vapour bubbles expand periodically to the upstream side of the test section with subsequent periodic oscillation in the inlet pressure.

Flow boiling instability due to flow reversal depends strongly on the location of boiling incipience along the channel. Kandlikar [23] discussed nucleation and flow instability in microchannels. He reported that the location of boiling incipience affects flow reversal and thus the oscillation in the measured parameters such as pressure and temperature. When nucleation occurs near the channel exit, the flow resistance in the back flow direction is higher and consequently no flow reversal occurs (stable flow). On the contrary, when nucleation occurs near the channel inlet, the flow resistance in the backflow direction is lower and thus flow reversal occurs (unstable flow).

Although flow reversal is very common in horizontal multi-microchannels, it also occurs in vertical flows. For example, Tuo and Hrnjak [24] investigated experimentally periodic reverse flow of R-134a in a multi-microchannel evaporator having 1 mm hydraulic diameter and 260 mm channel length. The fluid entered the microchannel vertically upward. They reported that, the periodic reverse flow resulted in (i) flow maldistribution, (ii) lower heat transfer coefficient due to dryout and (iii) higher pressure drop. Qi et al. [25] reported flow instability during flow boiling of liquid nitrogen in vertical micro diameter tubes of diameter 1.042 mm and 1.931 mm. In their experiments there was a mixing chamber at the exit of the tube (plenum). They observed small bubbles that nucleate, detach from the nucleation cavities and move along the tube. These bubbles were observed to accumulate in the outlet plenum and form vapour patches, which block the tube temporarily and this process occurred periodically. At these conditions, the oscillation amplitude in pressure drop, mass flux and wall temperature was 30 kPa, 2250 kg/m^{2}s and 2.9 – 9.4 K, respectively.

Heat Transfer

Collier and Thome [26] stated that flow boiling heat transfer mechanisms in large diameter tubes are dominated by nucleate boiling in bubbly and slug flow (low to intermediate vapour quality) and convective boiling in annular flow (at high vapour quality). In nucleate boiling, the heat transfer coefficient depends only on heat flux while in convective boiling the heat transfer coefficient depends only on mass flux and vapour quality.

In microchannels there is no common agreement on the dominant heat transfer mechanism(s). Some researchers [27, 28] reported nucleate boiling as a dominant heat transfer mechanism while some others [29, 30] reported convective boiling or convective-nucleate boiling as dominant mechanism(s). Peng and Wang [27] investigated flow boiling of de-ionized water in a rectangular stainless steel multi-microchannel evaporator. The channel has 0.65 mm hydraulic diameter, 0.86 aspect ratio (W/H) and 60 mm length. The liquid subcooling was varied from 40 to 70 K and the experimental system was an open loop. They reported that no bubbles were observed in the channel although the boiling curve was exhibiting fully developed nucleate boiling. They attributed this phenomenon to the fact that channel size was much smaller than the “minimum evaporating space” required for bubble growth. Additionally, they did not report any effect for mass flux and inlet subcooling. Steinke and Kandlikar [28] performed an experimental study on flow boiling of water in copper multi-microchannels of 0.207 mm hydraulic diameter, 1.08 aspect ratio (W/H) and 57.15 mm long. Mass flux ranged from 157 to 1782 kg/m^{2}s, heat flux from 5 to 930 kW/m^2. The inlet sub-cooling was 78 K. The local heat transfer coefficient was plotted versus local vapour quality as a function of heat flux for different mass flux values. For the lowest mass flux (157 kg/m^{2}s), the heat transfer coefficient decreased with increasing vapour quality for all heat flux values up to x ≈ 0.8 then remains almost constant. A clear heat flux effect was reported at this mass flux where the heat transfer coefficient increased with increasing heat flux. On the contrary, as the mass flux increased, the effect of heat flux disappeared and the value of the local quality at which the

heat transfer coefficient remains constant decreased. This behaviour was attributed by Steinke and Kandlikar [28] to the dominance of nucleate boiling regime. The insignificant effect of heat flux at high mass flux was attributed to the rapid bubble growth with annular slugs that could lead to flow reversal. Lee and Mudawar [29] investigated flow boiling characteristics of R134a in a multi-microchannel evaporator having 0.35 mm hydraulic diameter, 0.32 aspect ratio (*W/H*) and 25.3 mm length. The fluid entered the test section as a two phase mixture using a throttling valve and the inlet quality was varied from 0.001 to 0.25. The heat transfer coefficient was reported to decrease with increasing vapour quality. They concluded that nucleate boiling dominates only at low heat flux for x < 0.05 while annular film evaporation (convective boiling) dominates for x > 0.05. Kosar et al. [30] investigated flow boiling of water in silicon rectangular microchannels with a hydraulic diameter 0.227 mm and 7.5 μm re-entrant cavities on the side walls. At the entrance of each channel a 20 μm wide orifice was installed. Based on the effect of heat and mass flux, they concluded that nucleate boiling dominates only at low mass flux (all heat flux values) and intermediate mass flux (low heat flux values). Convective boiling dominates only at high mass flux (all heat flux values) and intermediate mass flux (high heat flux values).

The above review indicates that there is no common conclusion about the dominant heat transfer mechanism(s) and the effect of heat and mass flux. Also, flow instability is a critical issue that should be highlighted in every boiling experiment. Thus, more research is still required in order to clarify and understand these fundamental points. The objective of the present study is to investigate the effect of heat and mass flux on flow boiling characteristics of de-ionized water in a single rectangular channel made of oxygen free copper. Flow visualization and instability are also investigated.

EXPERIMENTAL SETUP AND DATA REDUCTION

Figure 1 depicts a schematic drawing of the experimental facility. The system consisted of a reservoir, a sub-cooler, a magnetically coupled gear pump (Micropump GA-T23, PFSB), ultrasonic flowmeter (Atrato 710-V20-D) with an accuracy of ± 1% of the reading, preheater, test section and a condenser. A separate refrigeration system (not shown in the figure) was used for cooling the condenser and the sub-cooler. The de-ionized water was degassed in the reservoir by vigorous boiling for approximately one and half hour. The non-condensable gases were released to the ambient by opening the valve located on top of the condenser. The de-gassed water was then pumped to the test section and the fluid inlet temperature was controlled using a preheater and a PID controller. Two fine mesh filters (1 mm and 15 μm) were installed in the system to remove any particles in the water.

The single microchannel used in this study was tested first by Mirmanto et al. [31] for high mass flux range 600 – 1005 kg/m^{2}s. In this study the low mass flux range was considered. The test section was made of an oxygen-free copper block with dimensions, 1 mm width (*W*), 0.39 mm height (*H*) and 62 mm length (*L*) resulting in 0.56 mm hydraulic diameter and 2.56 aspect ratio (*W/H*). Figure 2 depicts the details of the test section. The average surface roughness (*Ra*) of the bottom surface of the microchannel was measured using a Zygo NewView 5000 surface profiler. The *Ra* value was measured near the channel inlet, the middle and the outlet and the value was respectively 0.601 μm, 0.450 and 0.387 μm. The test section was heated using one cartridge heater (Elmatic 600 W) inserted below the channel in a direction parallel to the flow. The heater has the same length as the test section to provide uniform heating. Six holes were drilled inside the copper block at 1.1 mm distance below the channel bottom to accommodate 6 K-type thermocouples to measure the local axial wall temperature. The top cover was made of a transparent polycarbonate material to enable flow visualization. The fluid inlet and outlet temperature was measured using K-type thermocouples. All thermocouples were calibrated during the present study with an uncertainty of ± 0.3 K. The pressure drop was measured directly using a differential pressure transducer (Omega PX409-015DWU) which was calibrated with an uncertainty value of ± 0.4 kPa. All data were recorded at a frequency of 1 kHz for 3 min using NI-compact modular data acquisition system with Labview software. Flow patterns were observed with a high-speed, high-resolution camera (Phantom V6) which was located on top of the test section. The camera was integrated with a stereo microscope (Huvitz HSZ-600) for better flow visualization.

Data Reduction

The heat loss from the test section was estimated by applying an electrical power (*P*) to the test section when there is no fluid inside. The temperature difference between the bottom wall and the ambient was recorded for each heating power after attaining steady state. The applied power was then plotted versus this temperature difference and the data were fitted to get an equation to calculate the heat loss (Q_{loss}) during boiling experiments. In other words, the temperature difference between the test section bottom wall and the ambient during an actual experiment was used to assess the Q_{loss}. The percentage of the heat loss varied from 5.2 to 9.2% over the experimental range. The heat flux (q'') was defined as:

$$q'' = \frac{P - Q_{loss}}{A_{ht}} \quad (1)$$

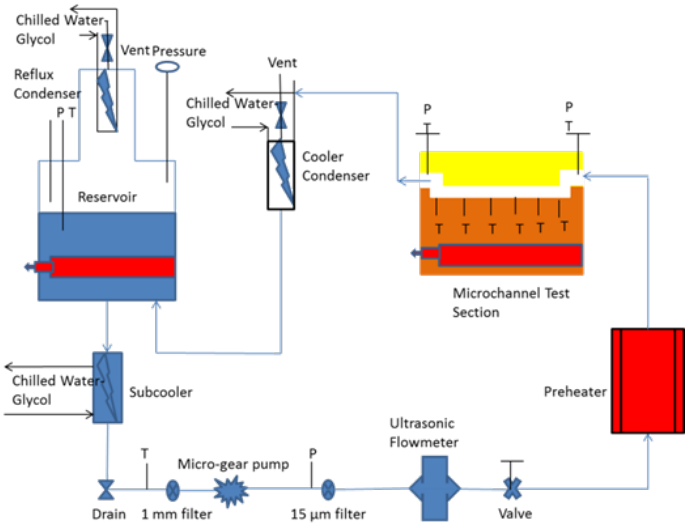

Figure 1: Schematic view of the experimental facility

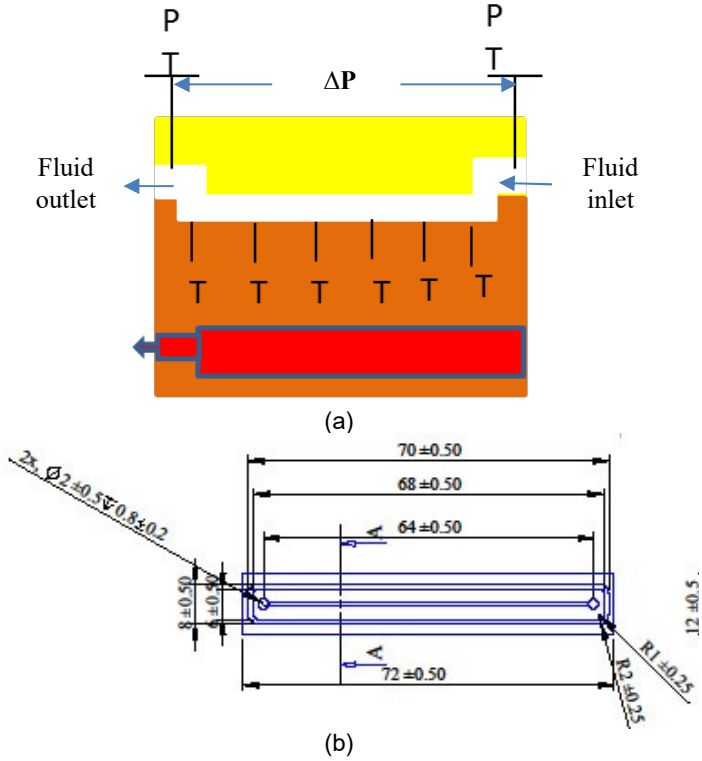

Figure 2: Test section details (a) front view, (b) dimensions of the test section in mm, Mirmanto et al. [31].

where A_{ht} is the heat transfer area, which is defined below as:

$$A_{ht} = (2\eta H + W)L \quad (2)$$

The top cover was assumed to be adiabatic and the heat flux was assumed to be uniform in the axial and transverse direction of the channel on all three walls. For a fin with an adiabatic tip, the fin efficiency (η) was defined as:

$$\eta = tanh(mH)/H \quad (3)$$

$$m = \sqrt{h/(k_{cu}t_{fin})} \quad (4)$$

The fin efficiency is nearly 0.995 for the present test section.

Single phase flow: The local single phase heat transfer coefficient $h_{sp}(z)$ and average Nusselt number *Nu* are calculated as:

$$h_{sp}(z) = \frac{q''}{T_w(z) - T_f(z)} \quad (5)$$

$$Nu = \frac{1}{L}\int_0^L \frac{h_{sp}(z)D_h}{k_l} dz \quad (6)$$

where, the channel wall temperature at axial location z corrected using the 1D heat conduction equation as given by eqn. (7) below. D_h, k_l and $T_f(z)$ are calculated by eqn. (8) below based on energy balance assuming uniform heat flux boundary condition.

$$T_w(z) = T_{tc}(z) - \frac{q''t}{k_{cu}} \quad (7)$$

$$T_f(z) = T_i + \frac{q''Wz}{\dot{m}c_p} \quad (8)$$

In the above equations, the distance from the channel bottom to the thermocouple location (t) is 1.1 mm. The single phase fanning friction factor f is calculated as:

$$f = \frac{\rho_l D_h \Delta P_{ch}}{2LG^2} \quad (9)$$

The channel pressure drop is calculated as:

$$\Delta P_{ch} = \Delta P_{meas} - \Delta P_{loss} \quad (10)$$

ΔP_{loss} is defined by eqn. (11) below is the pressure loss due to the inlet and outlet manifolds and the sudden contraction and enlargement.

$$\Delta P_{loss} = 2\left(\frac{1}{2}\rho_l V_p^2 K_{90}\right) + \frac{1}{2}\rho_l V_{ch}^2 (K_c + K_e) \quad (11)$$

K_{90}, K_c and K_e values were taken from Shah and London [32]. The flow enters and leaves the channel in a direction normal to the flow direction.

Two phase flow: Since the fluid enters the channel as a sub-cooled liquid, the channel is divided into a single phase region and a two phase region. The single-phase region starts from the channel inlet to the location of zero thermodynamic quality with length L_{sub}. Thus, the length of the two phase region becomes $L_{sat} = L - L_{sub}$. The length of the single-phase region L_{sub} is calculated iteratively using eqns. (12-14).

$$L_{sub} = \frac{\dot{m} c_p (T_{sat} - T_i)}{q''(2H+W)} \quad (12)$$

$$P_{sat}(L_{sub}) = P_i - \frac{2 f_{app} G^2}{\rho_l D_h} L_{sub} \quad (13)$$

$$f_{app} = \frac{3.44}{Re\sqrt{L^*_{sub}}} + \frac{(f_{FD}Re) + \frac{K(\infty)}{4L^*_{sub}} - \frac{3.44}{\sqrt{L^*_{sub}}}}{Re(1+C(L^*_{sub})^{-2}} \quad (14)$$

f_{app} is the apparent friction factor that was taken from Shah [33]. The values of the constant C, $f_{FD}Re$, and $K(\infty)$ in eqn. (14) are given in Shah [33] for rectangular channels. The dimensionless length L^*_{sub} in eqn. (14) is defined as:

$$L^*_{sub} = L_{sub}/(Re\, D_h) \quad (15)$$

The local pressure in the two-phase region was assumed to decrease linearly with the axial distance z and it can be calculated as:

$$P_{sat}(z) = P_{sat}(L_{sub}) - \frac{z - L_{sub}}{L - L_{sub}} \Delta P_{tp} \quad (16)$$

where the net two phase pressure drop across the channel is defined as:

$$\Delta P_{tp} = \Delta P_{ch} - \Delta P_{sp} \quad (17)$$

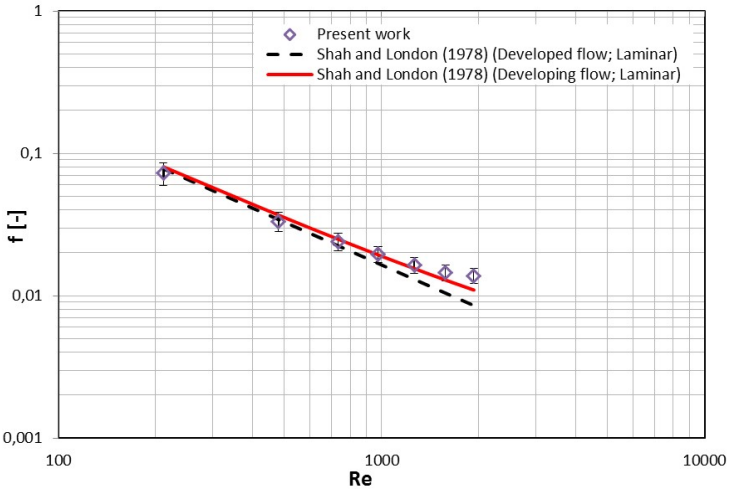

(a)

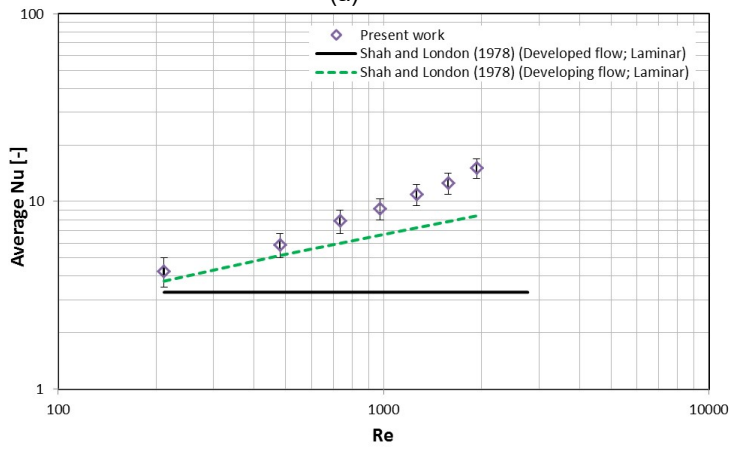

(b)

Figure 3: Single-phase validation, (a) f-Re, (b) Average Nu-Re

The single phase pressure drop part ΔP_{sp} in the above equation is calculated based on the length of the single phase region L_{sub} calculated using eqns. (12-14) and the apparent friction factor defined by eqn. (14). The local two phase heat transfer coefficient was defined as:

$$h_{tp}(z) = \frac{q''}{(T_w(z) - T_{sat}(z))} \quad (18)$$

The local saturation temperature in the above equation is calculated based on the local pressure given by eqn. (16) above. The thermodynamic mass quality was computed using eqns. (19) and (20) below.

$$i(z) = i_i + \frac{q''(2H+W)z}{\dot{m}} \quad (18)$$

$$x(z) = \frac{i(z) - i_l(z)}{i_{lg}(z)} \quad (19)$$

i_i is calculated based on the measured P_i and T_i. The experiments were conducted over a mass flux range 200 – 800 kg/m^{2}s. In the tests, the mass flux was kept constant and the heat flux was increased gradually in small steps. The propagated uncertainty analysis was conducted according to the method explained in Coleman and Steel [34] and the average values were 6.3 % for h_{sp}, 10.2 % for the fanning friction factor and 5.2 % for h_{tp}. The experimental set up was validated using single phase experiments. The single phase friction factor and Nusselt number compared with the Shah and London [32] correlations are depicted in Fig. 3. The figure demonstrates that there is a reasonable agreement between the measured and predicted values.

RESULTS AND DISCUSSION

Boiling Incipience Instability

Figure 4 depicts the fluctuations in the fluid inlet temperature, fluid outlet temperature, wall temperature and pressure drop for G = 200 kg/m^2 s. Figure 4(a, b) displays the signals at zero heat flux (before applying heat to the test section) and indicates very stable signals with insignificant fluctuations. The amplitude of fluctuations were 0.10 K, 0.06 K, 0.1 K and 0.31 kPa for the fluid inlet, outlet and wall temperature and pressure drop, respectively. When the heat flux was increased to 64.9 kW/m^2, boiling started and small bubbles were observed inside the channel. At this condition, the signal demonstrated large periodic fluctuations as seen in Figure 4(c, d). The fluctuations amplitude for the inlet, outlet and wall temperatures and pressure drop signal were 5 K, 4.5 K, 0.1 K and 3.9 kPa respectively. As the heat flux increased, the periodic nature of the signal disappeared and non-periodic fluctuations were observed for all heat flux values. Additionally, after boiling incipience, the fluctuations in fluid inlet temperature was higher than that in the outlet temperature. The wall temperature does not show significant fluctuations where the amplitude was about 0.3 K.

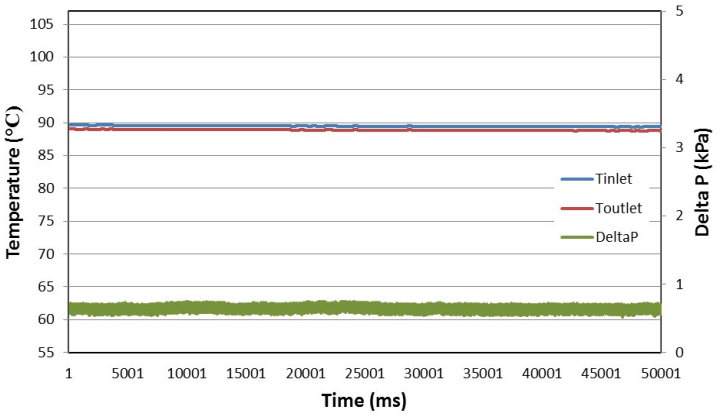

(a) Fluctuations in T_{inlet}, T_{outlet} and ΔP at q''= 0 kW/m^2

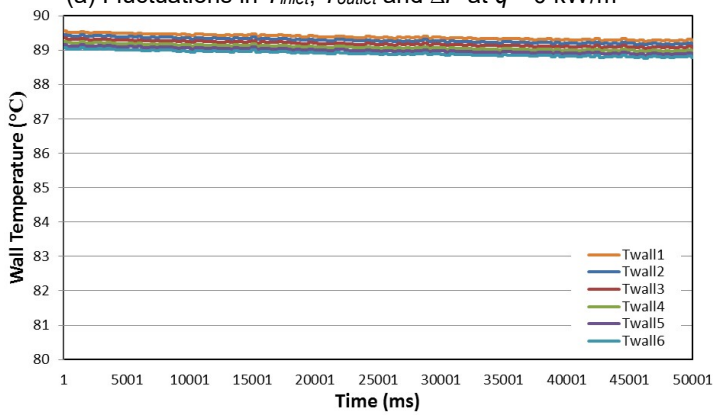

(b) Fluctuations in T_{wall} at q"= 0 kW/m^2

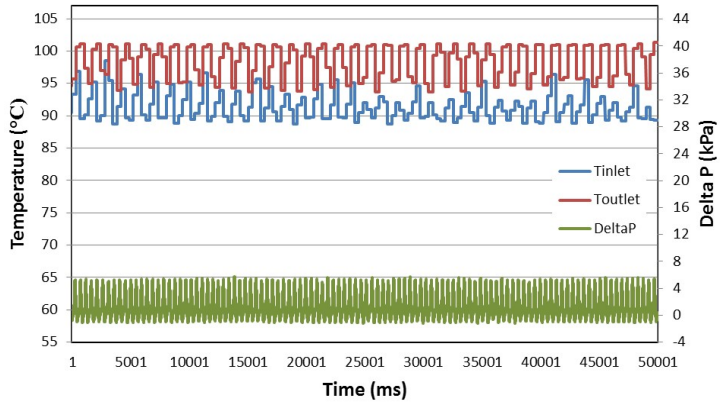

(c) Fluctuations in T_{inlet}, T_{outlet} and ΔP at q''= 64.9 kW/m^2

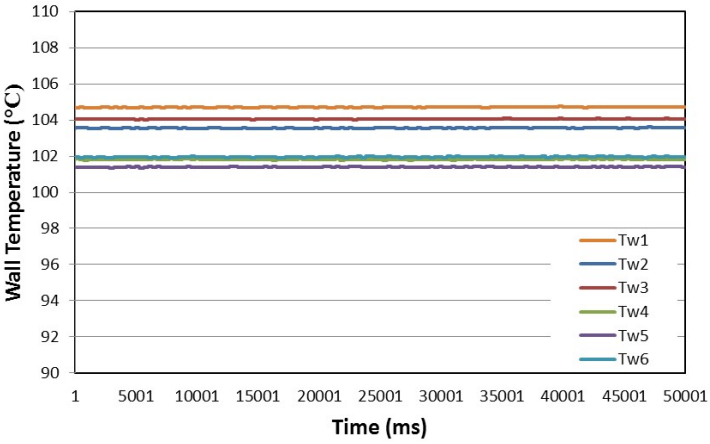

(d) Fluctuations in T_{wall} at $q"$= 64.9 kW/m^2

Figure 4: Fluctuations in fluid inlet, outlet and wall temperature and pressure drop at boiling incipience heat flux at G = 200 kg/m^{2}s

As the mass flux increases, the fluctuations in the above mentioned parameters were only observed at boiling incipience and became insignificant as heat flux increases. For example, Fig. 5 depicts the fluctuations recorded at boiling incipience for G = 400 kg/m^{2}s. When boiling started at $q"$ = *99* kW/m^2, significant fluctuations in the temperatures and pressure drop were recorded. The fluctuations amplitude at this condition was 2 K, 5 K, 0.1 K and 5 kPa respectively for the inlet, outlet and wall temperature and pressure drop. Analyzing the pictures captured using the high speed camera at boiling incipience indicated flow reversal, as seen in Fig. 6 for G = 400 kg/m^{2}s as an example. The flow reversal can also be detected from the pressure drop signal in Figs. 4 and 5 where the signal shows negative values.

The flow visualization was conducted at three locations along the channel, near the channel inlet, at the middle and near the channel outlet. Figure 6 displays the periodic evolution of flow patterns at boiling incipience for G = 400 kg/m^{2}s at the middle of the channel. The freehand sketch (red lines) indicates the boundaries of the bubbles to clarify the visualization. The figure demonstrates that small bubbles nucleate at the channel corners at time designated as t = 0 ms. After 5 ms, one bubble grew and spanned the channel width with smaller bubbles still observed at the channel edges. After 6 ms, the big bubble merged with the small bubbles and an elongated bubble was formed. The tail of this elongated bubble seems deformed (no spherical shape) while the nose of this bubble is not shown in the picture, see Fig. 6 (t = 7 ms). This picture shows also another bubble with a spherical head coming from the inlet region. These pictures demonstrate that bubbles nucleate, grow and merge rapidly before departure from the nucleation sites. This results in the formation of an elongated bubble which expands rapidly in the upstream and downstream sides of the channel.

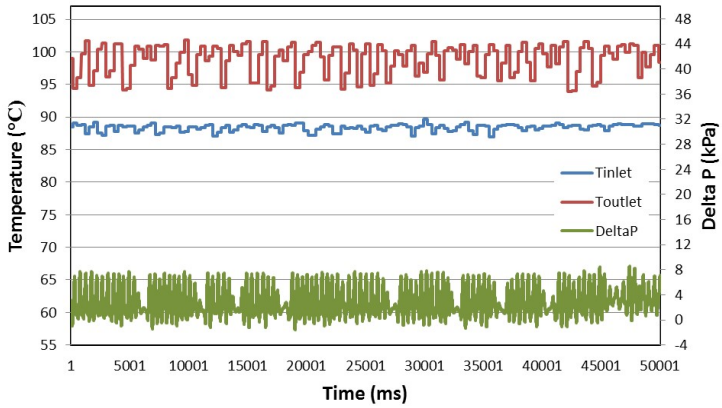

(a) Fluctuations in T_{inlet}, T_{outlet} and ΔP at $q"$= 99 kW/m^2

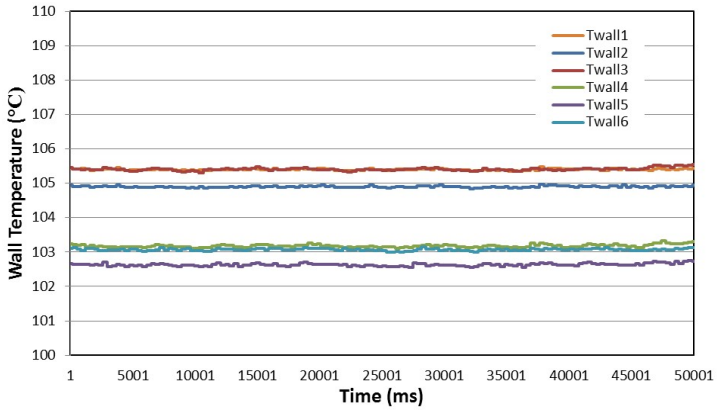

(b) Fluctuations in T_{wall} at $q"$= 99 kW/m^2

Figure 5: Fluctuations in fluid inlet, outlet and wall temperature and pressure drop at boiling incipience heat flux at g = 400 kg/m^2 s

The nose of the bubble moves faster than the tail. This could be attributed to the partial blockage of the channel resulting from the rapid growth of the bubble without departure from the nucleation site. Thus, the quantity of liquid in the downstream side of the channel becomes smaller compared to the upstream side. Given that the heat flux is constant, this can result in higher evaporation rate downstream of the bubble (thin liquid film have less thermal resistance). The pictures indicate also that the tail of the bubble moves slowly towards the channel inlet (back flow) until another bubble comes from the entry region of the channel. After 9 ms, the picture shows “annular-like” flow patterns but it is not annular flow. This pattern resulted from the coalescence of elongated bubbles. Additionally, this “annular-like” flow pattern was prevailing when the camera was moved to a location near the channel inlet and outlet. It is interesting to note that, after 32 ms, fresh liquid entered the channel and small

bubbles were observed to nucleate near the channel corners. This means that there is a periodic evolution of these flow patterns and the period is 32 ms for this mass flux. This behaviour was also observed for all mass fluxes but the period decreased with increasing mass flux, i.e. 68 ms for G = 200 kg/m^{2}s, 32 ms for G = 400 kg/m^{2}s, 21 ms for G = 600 kg/m^{2}s and 14 ms for G = 800 kg/m^{2}s.

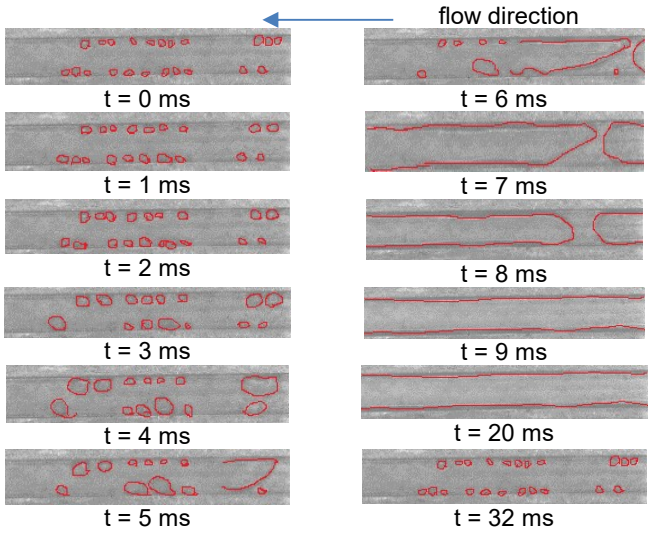

Figure 6: Sequence of flow images at the middle of the channel at boiling incipience for t_{in} = 89 °c, g = 400 kg/m^{2}s and q" = 99 kw/m^2

Heat Transfer Results

Figure 7 shows the effect of heat flux on the local heat transfer coefficient plotted versus local vapour quality (*h-x*) and axial distance (*h-z*) for G = 200 kg/m^{2}s at low heat flux values. As seen in the figure, boiling started near the middle of the channel (see the sudden increase in the heat transfer coefficient) with a clear small heat flux effect in the region near the channel exit. This could be interpreted as nucleate boiling dominant mechanism. The small heat flux effect observed at the lowest heat flux could be attributed to the absence of local dryout during the nucleation cycle. As discussed above in Fig. 6, there is bubble nucleation, growth and expansion is periodic. During this process, the elongated bubble seems stagnant for a while before the fresh liquid pushes it to the downstream side. Thus, at low heat flux values, it is probable that the elongated bubble leaves the channel before the liquid film dries out. Note for q"= 135.6 kW/m^2 the last thermocouple shows a large decrease in the heat transfer coefficient indicating partial dryout at this location. For moderate and high heat flux values, the effect of heat flux became very complex and partial dryout is observed at the last thermocouple for all heat flux values. Figure 8 depicts the behaviour of the heat transfer coefficient at high heat flux values. It is obvious that the axial distance and the local quality plots show insignificant heat flux effect at very low quality values, x < 0.1. For higher quality values, the effect of heat flux was very small but the heat transfer coefficient decreases with increasing heat flux. This behaviour could be attributed to the rapid bubble growth and elongation along the channel at high heat flux, which might suppress the nucleation process. Additionally, the evaporation rate of the liquid film around the elongated bubble may be so high, such that dry patches might form underneath the bubble.

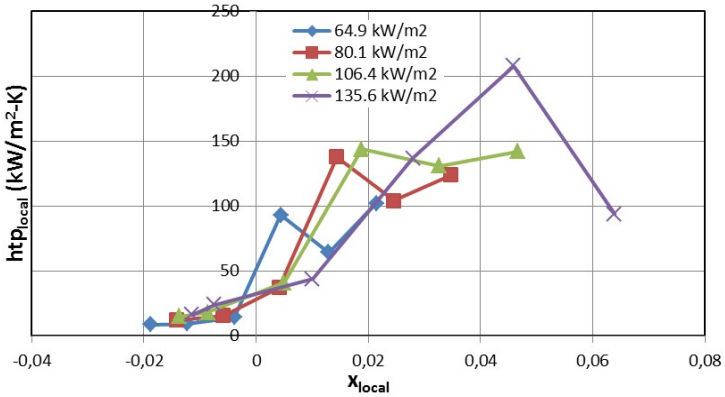

(a)

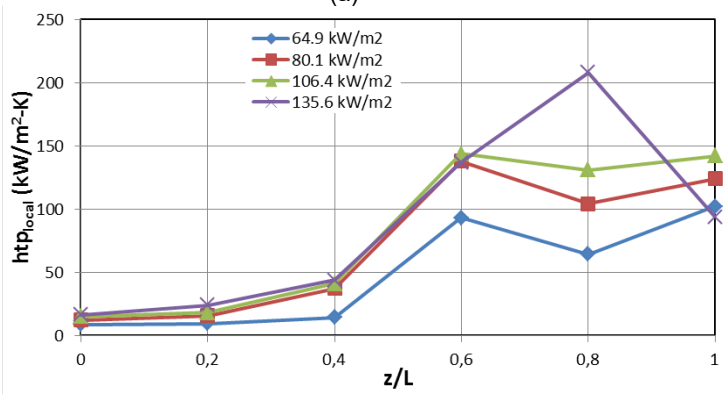

(b)

Figure 7: Effect of heat flux on the local heat transfer coefficient at low heat flux for g = 200 kg/m^{2}s, (a) h-x plot, (b) h-z plot

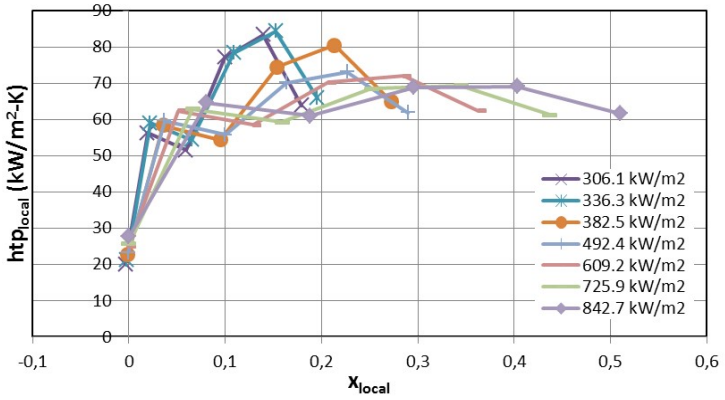

(a)

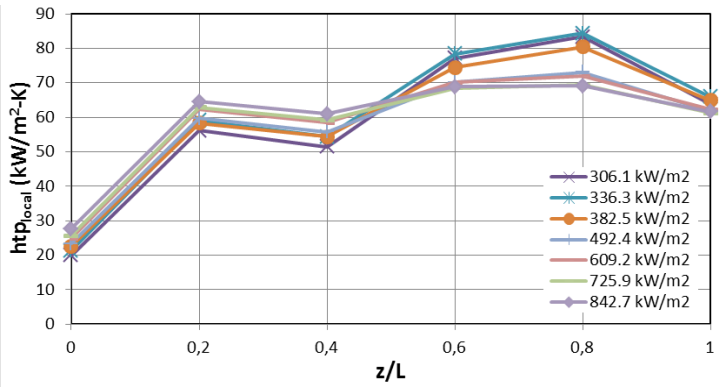

(b)

Figure 8: Effect of heat flux on the local heat transfer coefficient at high heat flux for g = 200 kg/m^{2}s, (a) h-x plot, (b) h-z plot

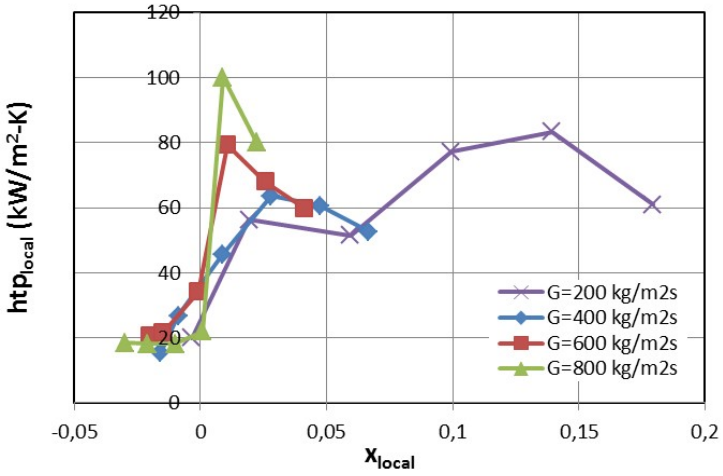

(a)

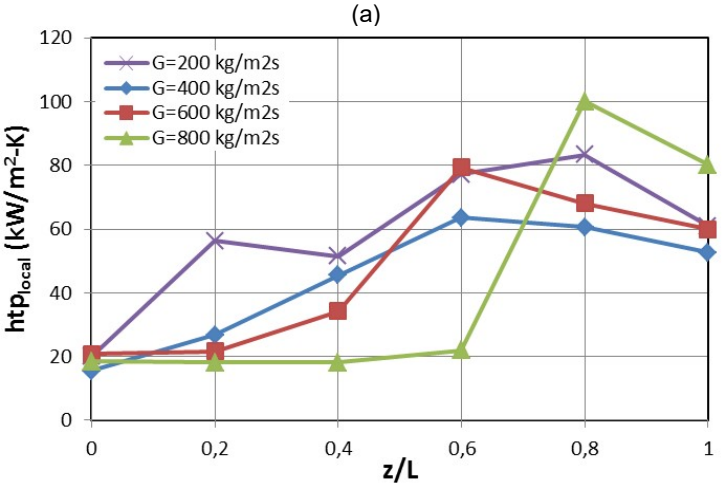

(b)

Figure 9: Effect of mass flux on the local heat transfer coefficient at low heat flux 293 kw/m^2, (a) h-x plot, (b) h-z plot

Figure 9 depicts the effect of mass flux on the local heat transfer coefficient plotted on the *h-x* and *h-z* plane at q = 293 kW/m^2. The figure demonstrates that the effect of mass flux on the local heat transfer coefficient at low heat flux is not clear, see Fig. 9 (a, b). At high heat flux values, (see Fig. 10), there is a clear mass flux effect in the very low quality region. However, the axial distance plot indicates that there is a clear mass flux effect over the second half of the channel (from the middle to the exit) where the heat transfer coefficient increased with increasing mass flux.

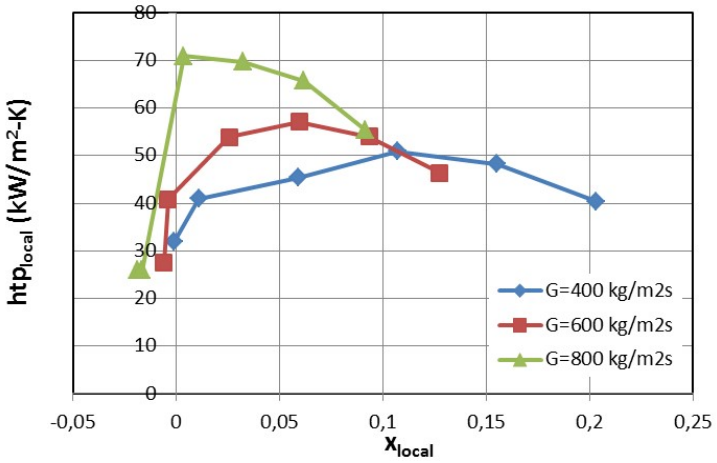

(a)

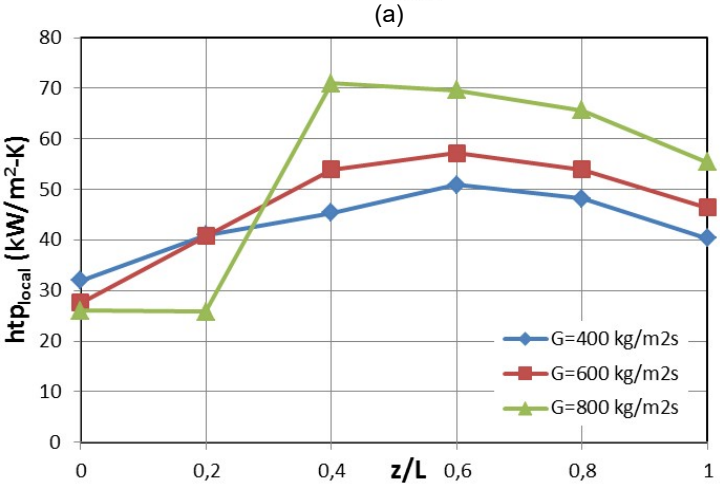

(b)

Figure 10: Effect of mass flux on the local heat transfer coefficient at low heat flux 697 kw/m^2, (a) h-x plot, (b) h-z plot

The heat transfer results presented in this section indicate very complex behaviour. This complexity makes it difficult to infer the dominant heat transfer mechanism(s) in this study. Some researchers [15, 28, 35-37] conducted flow boiling studies using water in microchannels and agreed on the trend of the local heat transfer coefficient versus local vapour quality, which was different compared to the present study. They agreed on that the heat transfer coefficient decreases rapidly from a peak value at x = 0 then decreases moderately with increasing vapour quality. However, there were contradictions in the mass and heat flux effects. Sobierska et al. [15] reported clear heat flux effect for all mass flux range (100 – 700 kg/m^{2}s) while Kandlikar and Steinke [28] reported heat flux effect only

for the lowest mass flux in their study (157 kg/m^{2}s). For higher mass flux values, Kandlikar and Steinke [28] did not see any heat flux effect and attributed this to the rapid bubble growth and flow reversal. Sobierska et al. [15] reported heat transfer coefficient that decreases with increasing mass flux. On the contrary, Galvis and Culham [35] reported that the heat transfer coefficient decreases with heat flux up to a certain heat flux value after which it shows small dependence on both heat and mass flux. However, they reported nucleate boiling as a dominant heat transfer mechanism. Lim et al. [37] did not find any mass flux effect over the quality range up to x = 0.2 with the heat transfer coefficient decreases with quality for x < 0.06 after which it remains constant. For G = 200, 400 kg/m^{2}s, the heat transfer coefficient was almost independent of heat flux. Increasing the mass flux to 600 kg/m^{2}s, the heat transfer coefficient decreased rapidly with heat flux up to a certain value then it decreased moderately.

CONCLUSIONS AND FUTURE WORKS

In this study, flow boiling experiments were performed in a single copper microchannel over a wide range of heat flux (56-865 kW/m^2) and mass flux (200-800 kg/m^{2}s). The main conclusions drawn from this study are:

- Flow visualization demonstrated that bubbles nucleate and rapidly grow without detaching from the nucleation cavity within the current experimental range. The rapid growth of the bubble before leaving the channel wall resulted in the formation of an elongated bubble, which blocks the channel temporarily (periodically). This periodic blockage results in the onset of flow boiling instability with large fluctuations in temperature and pressure.
- At boiling incipience, nucleation process including bubble growth into elongated bubbles occurred periodically. The period was detected from flow visualization through the sequence of pictures. The period was found to decrease with increasing mass flux, i.e. the elongated bubble can stay longer before leaving the channel at low mass flux. Thus there is a possibility of periodic partial dryout as mass flux decreases.
- There is a small heat flux effect only at low heat and mass flux values. At high heat and mass flux values, there was no heat flux effect.
- The heat transfer dominant mechanism is not clear in this study. A longer test section is needed in order to cover a wide range of vapour quality to help clarify the dominant heat transfer mechanism(s).

NOMENCLATURE

A_{ht}	Heat transfer area	[m^2]
c_p	Liquid specific heat	[J/kg°C]
D_h	Hydraulic diameter	[m]
f	Single-phase fanning friction factor	[-]
G	Mass flux	[kg/m^{2}s]
h	Heat transfer coefficient	[W/m^{2}K]
H	Height of the microchannel	[m]
i	Specific enthalpy	kJ/kg
K	Pressure loss coefficient	[-]
k	Thermal conductivity	[W/mK]
L	Length	[m]
m	Fin parameter	[-]
$\dot{m}$	Mass flow rate	[kg/s]
Nu	Nusselt number	[-]
P	Power	[W]
Q	Heat energy	[W]
q”	Heat flux	[W/m^2]
Ra	Average surface roughness	[µm]
Re	Reynolds number	
T	Temperature	[°C]
t	Thickness, time	[m], [ms]
V	Velocity of the liquid	[m/s]
W	Width of the microchannel	[m]
x	Thermodynamic mass vapour quality	[-]
z	Axial distance	[m]
Greek		
η	Fin efficiency	[-]
ρ	Density	[kg/m^3]
ΔP	Pressure drop	[Pa]
Subscripts		
app	Apparent	
c	Sudden contraction	
ch	channel	
cu	Copper	
e	Sudden enlargement	
f	Fluid	
FD	Fully developed	
fin	Fin	
i	Inlet	
l	liquid	
lg	Vapourization	
local	Local	
loss	Loss	
meas	measured	
p	Plenum	
sat	Saturation	
sp	Single-phase	
sub	Subcooled	
tc	Thermocouple	
tp	Two-phase	
outlet	Outlet	
w	wall	
90	Normal to the flow direction	

ACKNOWLEDGMENTS
The first author acknowledges the support provided by the Turkish Higher Research Council.

REFERENCES
[1] J. Lee, I. Mudawar, Fluid flow and heat transfer characteristics of low temperature two-phase micro-channel heat sink-part I: Experimental methods and flow visualization results, International Journal of Heat and Mass Transfer, 51 (2008) 4315-4326.
[2] S.G. Kandlikar, High flux heat removal with microchannels-A roadmap of challenges and opportunities, Heat Transfer Engineering, 26 (2005) 5-14.
[3] L. Consolini, J.R. Thome, Microchannel flow boiling heat transfer of R134a, R236fa and R245fa, Microfluidics and Nanofluid, 6 (2009) 731–746.
[4] T.G. Karayiannis, D. Shiferaw, D.B.R. Kenning, V.V. Wadekar, Flow pattern and heat transfer for flow boiling in small to micro diameter tubes, Heat Transfer Engineering, 31 (2010) 257 – 275.
[5] I. Mudawar, Two-phase microchannel heat sinks: theory, application and limitation, Journal of Electronic Packaging, 133 (2011) 1002-1033.
[6] Y. Daghighi Microfluidic technology and its biomedical applications, Journal of Thermal Engineering, 1 (2) (2015) 621-626.
[7] V.W. Bhatkar, V.M. Kriplani, G.K Awari, Experimental performance of R134a and R152a using microchannel condenser, Journal of Thermal Engineering, 1 (2) (2015) 575-582.
[8] J.A. Boure, A.E. Bergles, L. S. Tong, Review of two-phase flow instability, Nuclear Engineering Design, 25 (1973) 165-192.
[9] A.E. Bergles, S.G. Kandlikar, On the nature of critical heat flux in microchannels, Journal of Heat Transfer, 127 (2005) 101-107.
[10] M.M. Mohamed, T.G. Karayiannis, D.B.R. Kenning, Surface effects in flow boiling of R 134a in microtubes, International Journal of Heat and Mass Transfer, 54 (2011) 3334-3346.
[11] E.A. Pike-Wilson, T.G. Karayiannis, Flow boiling of R245fa in 1.1 mm diameter stainless steel, brass and copper tubes, Experimental Thermal and Fluid Sciences 59 (2014) 166–183.
[12] T.G. Karayiannis, M.M. Mahmoud, D.B.R. Kenning, A study of discrepancies in flow boiling results in small to micro diameter metallic tubes, Experimental Thermal and Fluid Sciences, 36 (2012) 126-142.
[13] J.R. Thome, Engineering Data Book III, Wolverine Tube Inc., 2004 (Chap. 12).
[14] S.G. Kandlikar, Two-phase flow patterns, pressure drop, and heat transfer during boiling in minichannel flow passages of compact evaporators, Heat Transfer Engineering, 23 (2002) 5 – 23.
[15] E. Sobierska, R. Kulenovic, R. Mertz, M. Groll, Experimental results of flow boiling of water in a vertical microchannel, Experimental Thermal and Fluid Sciences, 31 (2006) 111-119.
[16] A. Megahed, I. Hassan, Two-phase pressure drop and flow visualization of FC-72 in a silicon microchannel heat sink, International Journal of Heat and Fluid Flow, 30 (2009) 1171-1182.
[17] T. Chen, S.V. Garimella, Measurements and high-speed visualizations of flow boiling of a dielectric fluid in a silicon microchannel heat sink, International Journal of Multiphase Flow, 32 (2006) 957-971.
[18] K. Balasubramanian, M. Jagirdar, P.S. Lee, C.J. Teo, S.K. Chou, Experimental investigation of flow boiling heat transfer and instabilities in straight microchannels, International Journal of Heat and Mass Transfer, 66 (2013) 655-671.
[19] W. Qu, I. Mudawar, Measurement and prediction of pressure drop in two phase micro-channel heat sinks, International Journal of Heat and Mass Transfer, 46 (2003) 2737-2753.
[20] K.H. Chang, C. Pan, Two-phase flow instability for boiling in a microchannel heat sink, International Journal of Heat and Mass Transfer, 50 (2007) 2078-2088.
[21] D. Bogojevic, K. Sefiane, A.J. Walton, H. Lin, G. Cummins, Two-phase flow instabilities in a silicon microchannels heat sink, International Journal of Heat and Fluid Flow, 30 (2009) 854-867.
[22] G. Wang, P. Cheng, H. Wu, Unstable and stable flow boiling in parallel microchannels and in a single microchannel, International Journal of Heat and Mass Transfer, 50 (2007) 4297-4310.
[23] S.G. Kandlikar, Nucleation characteristics and stability considerations during flow boiling in microchannels, Experimental Thermal and Fluid Sciences, 30 (2006) 441-447.
[24] H. Tuo, P. Hrnjak, Periodical reverse flow and boiling fluctuations in a microchannel evaporator of an air-conditioning system, International Journal of Refrigeration, 36 (2013) 1263-1275.
[25] S.L. Qi, P. Zhang, R.Z. Wang, L.X. Xu, Flow boiling of liquid nitrogen in microtubes: part I - the onset of nucleate boiling, two-phase flow instability and two-phase flow pressure drop, International Journal of Heat Mass Transfer, 50 (2007) 4999-5016.
[26] J.G. Collier, J.R. Thome, Convective Boiling and Condensation, third ed., Oxford University Press, Oxford, 1994.
[27] X.F. Peng, B.X. Wang, Forced convection and flow boiling heat transfer for liquid flowing through microchannels, International Journal of Heat and Transfer, 36 (1993) 3421-3427.
[28] M.E. Steinke, S.G. Kandlikar, An experimental investigation of flow boiling characteristics of water in parallel microchannels, Journal of Heat Transfer, 126 (2004) 518-526.
[29] J. Lee, I. Mudawar, Two-phase flow in high-heat-flux micro-channel heat sink for refrigeration cooling

applications: part II-heat transfer characteristics, International Journal of Heat and Mass Transfer, 48 (2005) 941-955.
[30] A. Kosar, C.J. Kuo, Y. Peles, Boiling heat transfer in rectangular microchannels with reentrant cavities, International Journal of Heat and Mass Transfer, 48 (2005) 4867-4886.
[31] Mirmanto, D.B.R. Kenning, T.G. Karayiannis, J.S. Lewis, Pressure drop and heat transfer characteristics for single phase developing flow of water in rectangular microchannels, Journal of Physics: Conference Series, 395 (2012) 012085-012098.
[32] R.K. Shah, A.L. London, Laminar flow forced convection in ducts. In: Irvin TF, Hartnett JP (eds) Advances in Heat Transfer. Academic , New York, 1978, pp. 124 – 128.
[33] R.K. Shah, A correlation for laminar hydrodynamics entry length solution for circular and non-circular ducts, Journal of Fluids Engineering, 100, pp. 177 – 179, 1978.
[34] H.W. Coleman, W.G. Steele, Experimentation, Validation, and Uncertainty Analysis for Engineers, 3rd edition, John Wiley and Son, Inc., Hoboken, New Jersey, USA, 2009.
[35] E. Galvis, R.Culham, Measurements and flow pattern visualization of two phase flow boiling in single channel microevaporator, International Journal of Multiphase Flow, 42 (2012) 52-61.
[36] D. Liu, X. Weng, X. Xu, Experimental study on the heat transfer coefficient of water flow boiling in mini/microchannels, Experimental Thermal and Fluid Sciences, 35 (2011) 1392-1397.
[37] T-W. Lim, W-S. You, J-H. Choi, H-S. Kim, Experimental investigation of heat transfer in two phase flow boiling, Experimental Heat Transfer, 28 (2015) 23-36.